EUROPEAN ORGANIZATION FOR NUCLEAR RESEARCH

July 21, 1997

Study of the radiative decay Z$\rightarrow \tau^+\tau^-\gamma$ and limits on the anomalous magnetic and electric dipole moments of the tau

The L3 Collaboration

Abstract

We have analysed radiative $e^+e^- \rightarrow \tau\tau(\gamma)$ events using $100\,\mathrm{pb}^{-1}$ of data collected by the L3 experiment during the 1991-1995 LEP runs at the Z resonance. The energy spectrum of the photons is compared to the predictions of QED including additional anomalous magnetic and electric dipole terms. No deviations from the standard model are observed and the following constraints are placed on the anomalous magnetic and electric dipole form factors of the tau:

$$\begin{aligned} F_2(q^2=0) &= -0.002 \pm 0.022 \pm 0.020 \\ eF_3(q^2=0) &= (-0.1 \pm 1.2 \pm 1.1) \times 10^{-16}\mathrm{e{\cdot}cm} \end{aligned}$$

These results are preliminary.

Submitted to *Intl. Europhysics Conference on High Energy Physics, Jerusalem '97*

1 Introduction

In the standard model, the charged leptons are identical in all respects except for their masses and distinct lepton numbers. There is, however, no experimentally verified explanation for why there are three generations of leptons nor for why they have such differing masses. New insight might be forthcoming if the leptons were observed to have substructure which could manifest itself in the value of the anomalous magnetic or electric dipole moments. The anomalous moments for the electron and muon are already measured with high precision and are found to be in excellent agreement with QED predictions [1]. Anomalous moments of the tau are relatively poorly known and are of particular interest since, as the heaviest lepton, the tau may exhibit the most sensitivity to new physics.

We have analysed data collected by the L3 detector at LEP during 1991–1995. The anomalous magnetic and electric dipole moments of the tau are measured using the energy spectrum of photons radiated in $\tau\tau$ events produced in e^+e^- collisions at $\sqrt{s} \approx m_Z$.

2 Anomalous electromagnetic moments in $\tau\tau\gamma$ events

In general a photon may couple to a tau through its electric charge, magnetic dipole moment, or electric dipole moment (neglecting possible anapole moments [2]), as shown schematically in figure 1 for taus produced in e^+e^- collisions. We may parametrise this coupling with the

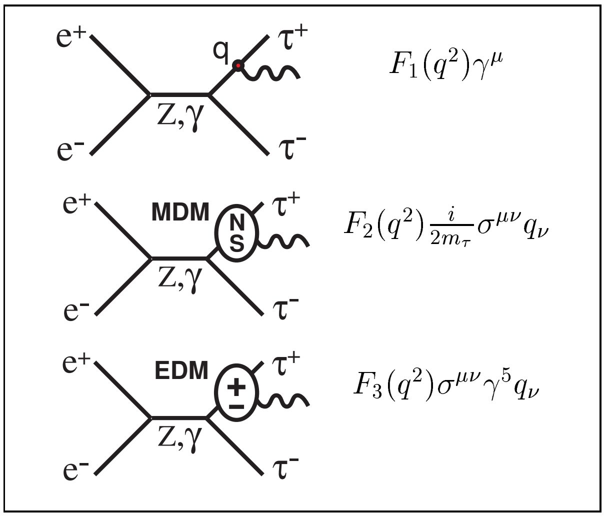

Figure 1: Photon couplings to a tau produced in an e^+e^- collision, induced by an electric charge (top), a magnetic dipole moment (centre), or an electric dipole moment (bottom).

matrix element

$$\langle \tau(p') | J_\mu | \tau(p) \rangle = \bar{u}(p') \Gamma_\mu u(p). \tag{1}$$

Γ_μ represents the most general Lorentz-invariant form of the coupling of a tau to a photon of 4-momentum q_ν:

$$\Gamma^\mu = F_1(q^2)\gamma^\mu + F_2(q^2)\frac{i}{2m_\tau}\sigma^{\mu\nu}q_\nu - F_3(q^2)\sigma^{\mu\nu}\gamma^5 q_\nu. \tag{2}$$

The q^2-dependent form-factors, $F_i(q^2)$, have familiar interpretations for $q^2 = 0$:

$$F_1(q^2\!=\!0) \equiv q_\tau \quad \text{is the electric charge of the tau;}$$
$$F_2(q^2\!=\!0) \equiv a_\tau = (g-2)/2 \quad \text{is the static anomalous magnetic moment of the tau (where } g \text{ is the gyromagnetic ratio);}$$
$$F_3(q^2\!=\!0) \equiv d_\tau/q_\tau \quad \text{where } d_\tau \text{ is the static electric dipole moment of the tau.}$$

In the standard model, a_τ is non-zero due to loop effects. It has been calculated to be [3]

$$a_\tau = \alpha/2\pi + \ldots = 0.001\,177\,3(3). \tag{3}$$

A non-zero value of d_τ is forbidden by both P invariance and T invariance. Assuming CPT invariance, observation of a non-zero value of d_τ would imply CP violation in the τ system.

In order to ascertain the effects of electric and anomalous magnetic dipole moments on the $\mathrm{e^+e^-} \rightarrow \tau\tau\gamma$ cross section and photon energy and angular distributions, we have performed a calculation of the full squared matrix element for such events. Using the parametrisation of the electromagnetic current given in equation 2, we consider the standard model and anomalous amplitudes for the diagrams shown in in figure 2. In the evaluation of the matrix element from these amplitudes, both γ and Z exchange are considered, no interference terms are neglected and no fermion masses are set to zero. The calculation has been cross-checked against an independent approximate calculation [4], and is described in detail elsewhere [5].

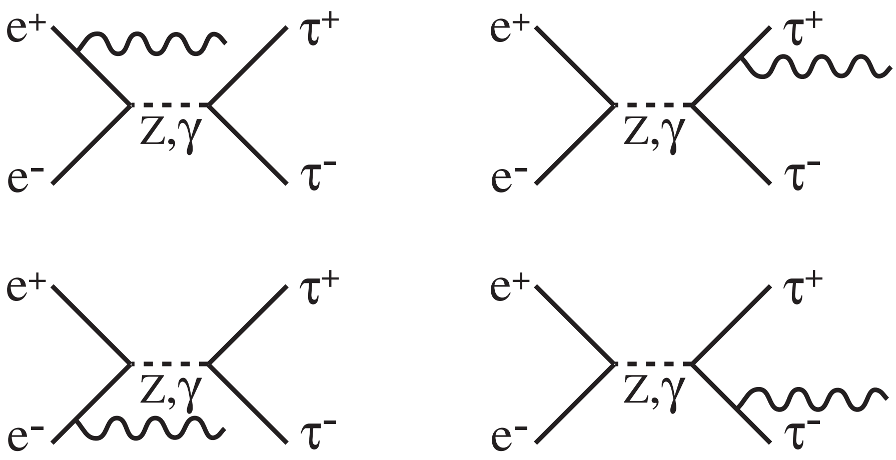

Figure 2: Tree-level Feynman diagrams for the process $\mathrm{e^+e^-} \rightarrow \tau^+\tau^-\gamma$.

3 The L3 detector

The L3 detector is described in detail elsewhere [6,7]. The central tracking chamber is a Time Expansion Chamber (TEC) consisting of two coaxial cylindrical drift chambers with 12 inner and 24 outer sectors. The Z-chamber surrounding the TEC consists of two coaxial proportional chambers with cathode strip readout. The electromagnetic calorimeter is composed of bismuth germanate (BGO) crystals. The energy resolution of the BGO for photons above 2.5 GeV, as selected in this analysis, is approximately 1.4%. Hadronic energy depositions are measured by a uranium proportional wire chamber sampling calorimeter surrounding the BGO. Scintillator time-of-flight counters are located between the electromagnetic and hadronic calorimeters. The muon spectrometer, located outside the hadron calorimeter, consists of three layers of drift chambers measuring the muon trajectory in both the bending and the non-bending planes. All subdetectors are installed inside a solenoidal magnet which provides a uniform field of 0.5 T.

4 Event selection

4.1 Selection of $\tau\tau(\gamma)$ events

The data sample used for this analysis corresponds to 100.05pb^{-1} collected at the Z peak. The selection of $\tau\tau(\gamma)$ events is restricted to barrel region, defined by $|\cos\theta_{\rm thrust}| < 0.743$ where $\theta_{\rm thrust}$ is the thrust axis of the event. Hadronic events are rejected by requiring small numbers of charged tracks and energy clusters. Two photon events are rejected by requiring that the event contains a total measured energy of more than $0.15\sqrt{s}$, where $\sqrt{s}$ is the centre-of-mass energy, and two jets each having at least $0.02\sqrt{s}$. No track acollinearity cut is applied since this would preferentially reject $\tau\tau$ events containing a high energy photon. Cosmic muons are rejected by requiring scintillator hits to be in time with the beam crossing and by rejecting events with no tracks pointing to the interaction region.

To reject Bhabha events we require that the energies of identified pairs of electrons should not exceed 35 GeV and 30 GeV for the highest energy and second highest energy electron respectively. Radiative Bhabha events are rejected by requiring that the total BGO energy does not exceed 70 GeV. Residual background from Bhabha events in which an electron is not explicitly reconstructed, for example due to a detector inefficiency, is reduced by rejecting events with more than 40 GeV in the BGO and less than 1 GeV in the Hadron Calorimeter.

To remove the background from $Z \to \mu^+\mu^-$, all events with two identified muons are rejected. Events with a single muon are rejected if that muon has an energy of more than 30(20) GeV for muons with hits in 3(2) layers of the muon chambers. Residual background from di-muons, in which there is only one poorly measured muon or no identified muons at all, is reduced by requiring that the energies deposited in the BGO and Hadron Calorimeter are not consistent with the minimum-ionising signature of muons. A sample of 66 969 candidate $\tau\tau(\gamma)$ events survive these cuts.

To determine the selection efficiency of $\tau\tau(\gamma)$ events we use a sample of approximately 1.8 million simulated events. These are generated with the KORALZ Monte Carlo program [8], which in turn uses TAUOLA [9] for τ decays and PHOTOS [10] for standard model photon radiation. The simulated events are passed through the GEANT-based L3 detector simulation program [11] which allows for the effects of energy loss, multiple scattering, interactions and decays in the detector material as well as time-dependent detector effects. These events are then reconstructed using the same algorithms as for the data. The $\tau\tau(\gamma)$ selection efficiency is 43.6% for the full solid angle. As a cross-check of the selection procedure, the data sample was used to evaluate the $\tau\tau(\gamma)$ cross-section at $\sqrt{s} \approx m_{\rm Z}$. The result obtained is $\sigma_{\tau\tau} = 1.453\,{\rm nb}$, which agrees with the ZFITTER [12] prediction of $\sigma_{\tau\tau} = 1.479\,{\rm nb}$ to within the systematic uncertainty on the selection efficiency.

4.2 Selection of photons in $\tau\tau(\gamma)$ events

Photon candidates are identified by a shower in the barrel region of the BGO with no associated track in the TEC. The transverse profile of electromagnetic showers in the BGO is considerably narrower than for hadronic showers. Photon candidates are therefore required to have a narrow shower profile which is statistically consistent with that of an electromagnetic shower.

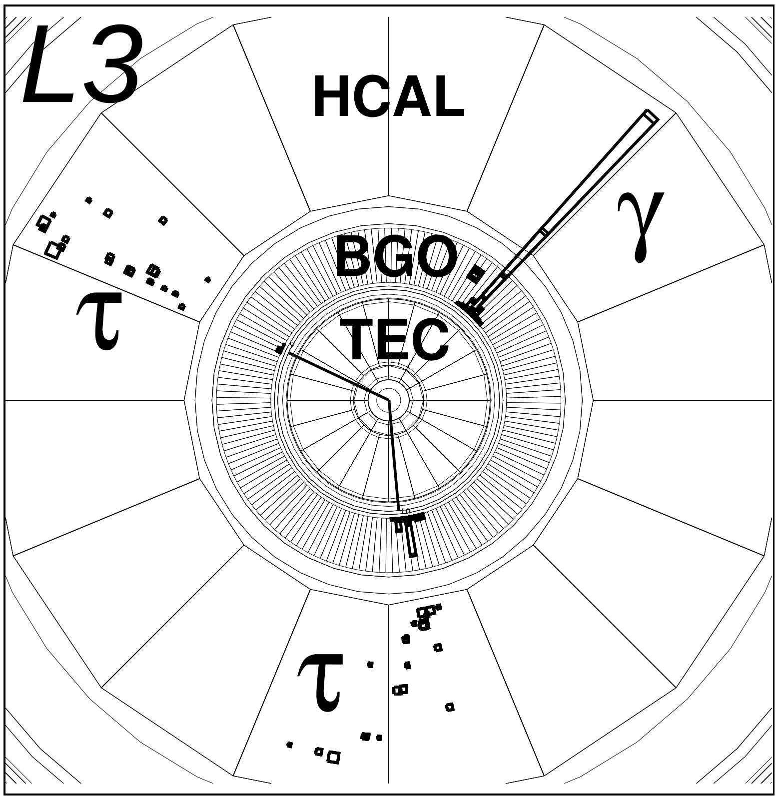

Figure 3: Typical $\tau\tau\gamma$ candidate event.

After applying these selection criteria, the sample of photon candidates consists of photons from initial and final state radiation as well as photons from $\pi^0 \to \gamma\gamma$ decays, photons radiated from τ decay products, and a small contribution from mis-identified decay products of the tau. Since the contribution to the energy spectrum due to anomalous tau moments is peaked at high energies, the energy of photon candidates is required to be greater than 2.5 GeV. Genuine photons from π^0 production in τ decays and fake photons from other mis-identified τ decay products tend to have small transverse energy with respect to τ direction. Most of this background is therefore removed by requiring the transverse energy of the photon to the nearest jet to be greater than 2.5 GeV.

After application of these cuts, 1265 events remain in the data which is consistent with the standard model expectation of 1305 events. The background consists predominantly of standard model initial and final state radiation photons from $\tau\tau(\gamma)$ events, with small contributions from Bhahbha events (2.4%), di-muon events (2.7%), and misidentified tau decay products (1.6%).

Figure 3 shows a typical $\tau\tau(\gamma)$ candidate event. The decay products of the taus in this event leave tracks in the TEC and energy in the BGO and hadron calorimeters. The photon has no associated track, leaves a considerable amount of energy in the BGO, and no energy in the hadron calorimeter. In addition to its distinctive signature, the photon is also well isolated from the decay products of the taus.

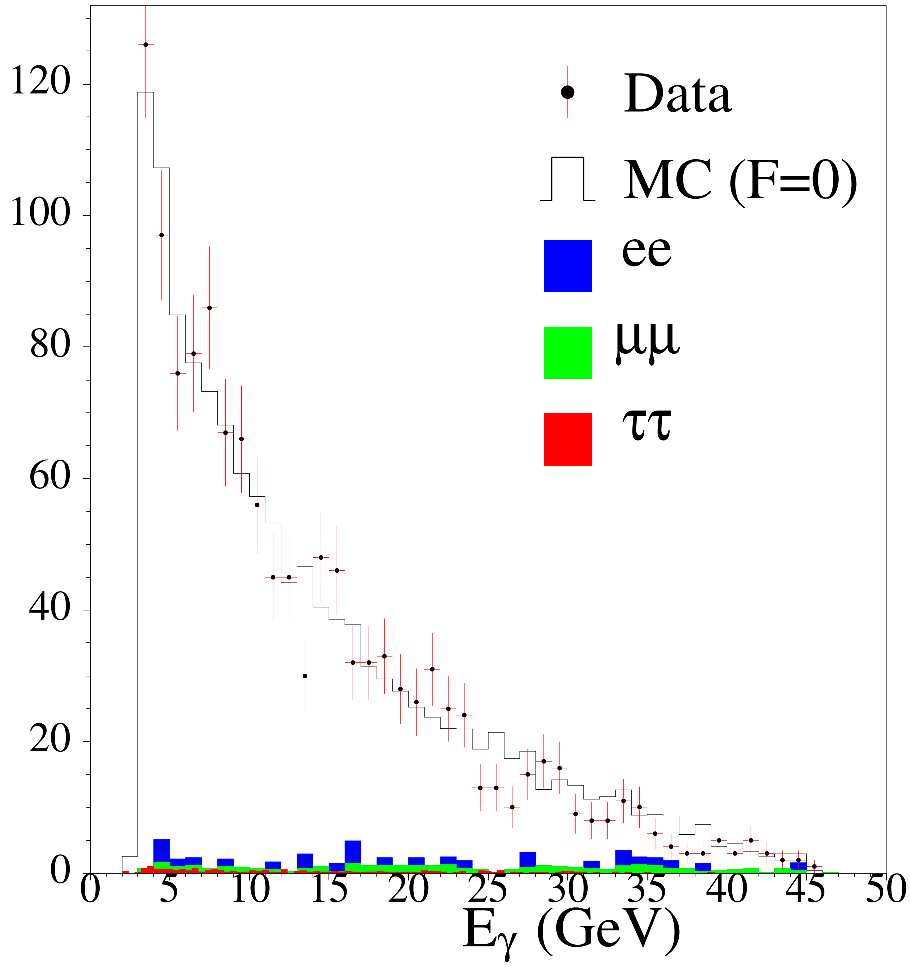

Figure 4: Energy spectrum of photons in selected $\tau\tau\gamma$ events. The data are denoted by points with error bars. The full histogram shows the predictions of the standard model, while the shaded histograms correspond to the contributions from Bhabha events, di-muon events, and tau decay products.

5 Preliminary results

To determine $F_2(q^2 = 0)$, a binned maximum likelihood fit is made to the measured photon energy spectrum. The standard model background contribution is estimated from the fully simulated $\tau\tau(\gamma)$, Bhabha, and di-muon Monte Carlo event samples, weighted according to the integrated luminosity of the data. The only free parameter in the fit is $F_2(q^2 = 0)$. The effect of $F_2(q^2 = 0)$ on the photon spectrum shape and absolute normalisation is determined as follows. The generator-level 4-vectors for each selected event in the $Z \to \tau^+\tau^-(\gamma)$ Monte Carlo sample are used to calculate the matrix element squared as a function of $F_2(q^2 = 0)$ using the methods described in section 2. The ratio of this matrix element squared to the standard model one is then used to weight the event for various $F_2(q^2 = 0)$ values. This makes it possible to accumulate histograms of photon energy spectra for many values of F_2.

Figure 4 shows the energy spectrum of selected photons for data (points with error bars) and the standard model Monte Carlo spectrum (full histogram). The likelihood as a function

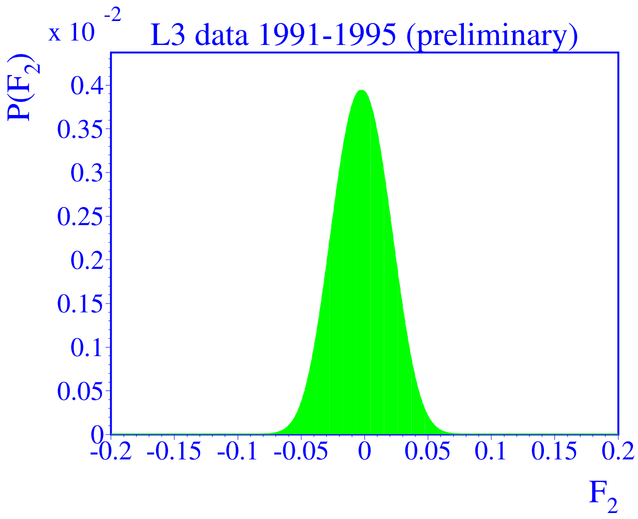

Figure 5: Likelihood as a function of F_2.

of $F_2(q^2 = 0)$ is shown in figure 5. The result of the fit is

$$F_2(q^2 = 0) = -0.002 \pm 0.022 \pm 0.020 \tag{4}$$

where the first error is statistical and the second error is systematic. The systematic error is dominated by efficiency uncertainties and the limited statistics of the Monte Carlo samples used to estimate the background. Alternatively $F_2(q^2 = 0)$ can be constrained to lie in the range:

$$-0.044 < F_2(q^2 = 0) < 0.039 \tag{5}$$

at the 95% confidence level.

Since no deviation from standard model expectations is observed in the photon energy spectrum, we may directly convert the constraint on $F_2(q^2 = 0)$ into a constraint on the electric dipole moment form factor, $F_3(q^2 = 0)$, by making the substitution $F_2(e/2m_\tau) \to eF_3$. The result is

$$eF_3(q^2 = 0) = (-0.1 \pm 1.2 \pm 1.1) \times 10^{-16}\text{e}\cdot\text{cm}. \tag{6}$$

6 Conclusions

We have placed the following constraints on the anomalous magnetic and electric dipole form factors of the tau,

$$\begin{aligned} F_2(q^2 = 0) &= -0.002 \pm 0.022 \pm 0.020 && (7) \\ eF_3(q^2 = 0) &= (-0.1 \pm 1.2 \pm 1.1) \times 10^{-16}\text{e}\cdot\text{cm} && (8) \end{aligned}$$

These results compliment those of other analyses [13, 14], which limit F_2 and F_3 at $q^2 \neq 0$. We note that the $q^2 = 0$ condition is necessary to associate these form factors with the static anomalous magnetic and electric dipole moments, a_τ and d_τ, of the tau. This preliminary result also significantly improves previously published limits on these two form factors at $q^2 = 0$ [15].

References

[1] E. R. Cohen and B. N. Taylor, Rev. Mod. Phys. **59** (1987) 1121.

[2] W. J. Marciano, (1990), Proceedings of the BNL Summer Study on CP Violation, Brookhaven National Laboratory, eds. S. Dawson and A. Soni.

[3] M. A. Samuel, G. Li and R. Mendel, Phys. Rev. Lett. **67** (1991) 668.

[4] J.Biebel and T. Riemann, (1996), DESY preprint DESY 96-112 (HEP-PH/961043).

[5] S. S. Gau, T. Paul, J. Swain and L. Taylor, (1997), Paper in preparation.

[6] L3 Collab., B. Adeva *et al.*, Nucl. Inst. Meth. **A 289** (1990) 35.

[7] L3 Collab., O. Adriani *et al.*, Physics Reports **236** (1993) 1.

[8] S. Jadach, B.F.L. Ward and Z. Wąs, Comp. Phys. Comm. **66** (1991) 276.

[9] S. Jadach, J.H. Kühn and Z. Wąs, Comp. Phys. Comm. **64** (1991) 275.

[10] E. Barberio, B. van Eijk and Z. Wąs, Comp. Phys. Comm. **66** (1991) 128.

[11] The L3 detector simulation is based on GEANT Version 3.15.
See R. Brun *et al.*, "GEANT 3", CERN DD/EE/84-1 (Revised), September 1987.
The GHEISHA program (H. Fesefeldt, RWTH Aachen Report PITHA 85/02 (1985)) is used to simulate hadronic interactions..

[12] D. Bardin *et al.*, FORTRAN package ZFITTER, and preprint CERN–TH. 6443/92;
D. Bardin *et al.*, Z. Phys. **C 44** (1989) 493;
D. Bardin *et al.*, Nucl. Phys. **B 351** (1991) 1;
D. Bardin *et al.*, Phys. Lett. **B 255** (1991) 290..

[13] D. J. Silverman and G. L. Shaw, Phys. Rev. **D27** (1983) 1196.

[14] R. Escribano and E. Massó, Phys. Lett. **B301** (1993) 419.

[15] J. A. Grifols and A. Méndez, Phys. Lett. **B255** (1991) 611, Erratum *ibid* B259 (1991) 512.